THE JOURNAL OF PHYSICAL CHEMISTRY Letters

Letter

pubs.acs.org/JPCL

Vibrational Dynamics of Interfacial Water by Free Induction Decay Sum Frequency Generation (FID-SFG) at the $Al_2O_3(1120)/H_2O$ Interface

Abdelaziz Boulesbaa and Eric Borguet*

Department of Chemistry, Temple University, 1901 North 13th Street, Philadelphia, Pennsylvania 19122, United States

Supporting Information

ABSTRACT: The dephasing dynamics of a vibrational coherence may reveal the interactions of chemical functional groups with their environment. To investigate this process at a surface, we employ free induction decay sum frequency generation (FID-SFG) to measure the time that it takes for free OH stretch oscillators at the charged (pH ≈ 13, KOH) interface of alumina/water (Al_2O_3/H_2O) to lose their collective coherence. By employing noncollinear optical parametric amplification (NOPA) technology and nonlinear vibrational spectroscopy, we showed that the single free OH peak actually corresponds to two distinct oscillators oriented opposite to each other and measured the total dephasing time, T_2, of the free OH stretch modes at the Al_2O_3/H_2O interface with a sub-40 fs temporal resolution. Our results suggested that the free OH oscillators associated with interfacial water dephase on the time scale of 89.4 ± 6.9 fs, whereas the homogeneous dephasing of interfacial alumina hydroxyls is an order of magnitude slower.

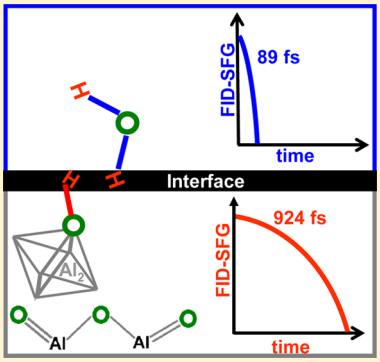

SECTION: Liquids; Chemical and Dynamical Processes in Solution

Due to the essential role that water plays in life, it has been and is still one of the most studied liquids.[1−3] Interfacial water, in particular, recently has become of special interest.[4] Water is interfaced with biomolecules in living cells,[2,3] minerals in soil,[5] metals in industry,[6] and semiconductors in photocatalysis.[7] In these environments, the formation and breaking of hydrogen bonding plays a major role in the interfacial reactivity.[8] In particular, at the interfaces of water with charged metal and semiconductor oxides terminated by hydroxyl groups, proton exchange via hydrogen bonding is most likely to occur.[9,10] In fact, it has been reported that at pH > 4, silanol groups (Si−OH) are deprotonated at the water/silica (H_2O/SiO_2) interface,[10] and at metal oxides surfaces, such as sapphire (α-$Al_2O_3(0001)$), at sufficiently low pH values, $(Al)_2OH$ groups can be protonated.[9] In order to understand these reactions, investigating the dynamics of hydrogen bonding network is indispensable. It has been reported that these dynamics are on the subpicosecond time scale in bulk water[11−13] and on the picosecond time scale in confined water systems.[14−16] The dynamics of water at solid interfaces still need insightful investigations.

Sum frequency generation (SFG) has become the technique of choice to investigate interfacial vibrational spectroscopy and dynamics.[17,18] Within the electric dipole approximation, SFG is forbidden in bulk water due to the presence of inversion symmetry.[19] However, this symmetry is broken at the interface, which makes SFG a suitable technique to study interfacial water due to its interface specificity.[4,19,20] In a typical vibrational SFG (vSFG) experiment, a spectrally broad mid-infrared (mid-IR) pulse, centered at a frequency ω_{IR}, coherently excites vibrational modes at the interface, and a second spectrally narrow pulse in the visible (ω_{Vis}), upconverts excited vibrational modes into an induced polarization in the visible centered at the sum frequency $\omega_{SFG} = \omega_{IR} + \omega_{Vis}$.[21] vSFG studies reported several vibrational modes of interfacial water in the 3000−4000 cm^{-1} frequency range; a low-frequency band centered at ∼3200 cm^{-1} assigned to strongly hydrogen bonded OH stretch modes, a middle-frequency band centered at ∼3450 cm^{-1} attributed to weakly hydrogen bonded OH stretch modes, and a high-frequency mode centered at ∼3700 cm^{-1} assigned to the free OH stretch mode.[19]

Recently, the interface of water with metal oxides, particularly alumina, has attracted the interest of several research groups.[6,9,22,23] The free OH vibrational mode centered at ∼3700 cm^{-1} is characteristic of the surface, which makes this mode a good choice to study for a better understanding of the interfacial water hydrogen bonding.[19] Although the peak centered at ∼3700 cm^{-1} in vSFG spectra has largely been assigned to the free OH stretch of H_2O,[19] at water/alumina interfaces such a consensus is not met. In fact, reports by the Shen and Dhinojwala groups have assigned the mode at ∼3700 cm^{-1} in vSFG at the water/$Al_2O_3(0001)$ interface to AlOH groups.[9,23,24] Furthermore, the shape of vSFG spectra from water/alumina interfaces seems to depend on the surface plane at which the alumina crystal was cut.[9,22] The vibrational mode at ∼3700 cm^{-1} in vSFG spectra was pronounced for alumina

Received: September 12, 2013
Accepted: November 26, 2013
Published: January 24, 2014

   dx.doi.org/10.1021/jz401961j | J. Phys. Chem. Lett. 2014, 5, 528−533

(0001)[9] but not in alumina ($1\bar{1}02$) interfaces.[22] Additionally, in the case of alumina ($1\bar{1}02$), a vibrational mode at ~3490 cm^{-1} was assigned to one type of hydroxyl group at the surface.[22] Could it be possible that the peak seen in the spectral region at ν > 3600 cm^{-1} in fact arises from both the AlOH hydroxyl group and the non-hydrogen-bonded OH stretch of interfacial water?

Often, vSFG spectral resolution is constrained by the width of the upcoverting pulse and detection systems, limiting the ability of the technique to reveal spectrally hidden vibrational transitions due to their narrow line width and/or coupling with neighboring oscillators.[17,18] This limitation may be overcome if vSFG experiments are carried out in the time domain, i.e., free induction decay vSFG (FID-SFG), with the condition that time domain measurements have higher temporal resolution compared to the vibrational dynamics of the interface. Additionally, time domain vSFG is more sensitive to inhomogeneous broadenings simultaneously present in frequency domain vSFG spectra.[25] In a typical vibrational FID-SFG experiment, a short IR pulse coherently excites vibrational oscillators and creates an initial state of vibrational coherence. Then, at a controlled time delay, $\Delta\tau$, a second short pulse probes the remaining coherence by generating a sum frequency polarization. The FID-SFG technique was reported for the first time by Guyot-Sionnest in 1991 in a study of the vibrational dynamics of the Si−H bond on a silicon (111) surface.[26]

With increasing developments in the technology of noncollinear optical parametric amplifiers (NOPAs),[27−30] ultra-broadband laser pulses capable of covering the various stretching vibrational modes of water with one acquisition have become available.[27,31] These ultra-broad-band laser pulses, when they are temporally compressed to the Fourier transform limit (FTL), are excellent tools for time-resolved experiments.[27,32] Here, we report on the measurement of coherence dynamics of the free OH stretch vibration at a charged $Al_2O_3(1120)/H_2O$ interface (pH ≈ 13, KOH). We employ vSFG in the frequency domain to reveal the nature of the vibrational modes at the investigated interface and NOPA technology to generate spectrally broad mid-IR and NIR pulses to carry out FID-SFG measurements with ~40 fs temporal resolution, sufficient to resolve the vibrational dynamics of the interfacial free OH vibrational stretch.

In order to reveal the vibrational modes at the charged interface of alumina/water, we measured the frequency domain Vis-SFG spectrum. The spectrum (symbols) shown in Figure 1 is normalized by dividing the Vis-SFG spectrum obtained at the Al_2O_3/H_2O interface by the Vis-SFG spectrum obtained at the Al_2O_3/Au interface. It shows two apparent bands, a low-frequency band at ~3200 cm^{-1} representing a strongly hydrogen bonded OH stretch[6,9,22−24] and a high-frequency band at ~3660 cm^{-1} indicating a free OH stretch mode.[6,9] The strongly hydrogen bonded OH stretch peak at this interface is red-shifted compared to that at the calcium fluoride/water interface (dashed plot in Figure 1), and the weakly hydrogen bonded OH stretch peak did not appear. To fit the normalized Vis-SFG spectrum at the Al_2O_3/H_2O interface, the well-known equation that describes the SFG process by a broad-band infrared pulse and a visible pulse is used.[17−19]

$$I_{\text{Vis-SFG}} \propto \left| \sum_n \frac{A_n}{\omega_{\text{mid-IR}} - \omega_n + i(\Gamma_n + \Delta\omega_{\text{Vis}}/2)} + |A_{\text{NR}}|e^{i\varphi} \right|^2 \quad (1)$$

where A_{NR}, φ, A_n, and Γ_n are the vibrationally nonresonant susceptibility amplitude, the phase between the resonant and nonresonant contributions, and the amplitude and damping constant of the surface vibration with frequency ω_n, respectively; $\omega_{\text{mid-IR}}$ and $\Delta\omega_{\text{Vis}}$ are the driving mid-IR pulse frequency components and the bandwidth of the upconverting visible pulse, centered at 800 nm, respectively.

Several reports have assigned low-frequency peaks (ν < 3300 cm^{-1}) in vSFG spectra of interfacial water to a strongly hydrogen bonded OH stretch.[9,23,24] Consequently, the peak centered at 3165.6 cm^{-1} in Figure 1 is assigned to strongly hydrogen bonded OH stretch modes. However, the high-frequency peak (ν > 3600 cm^{-1}) was not always assigned to the free OH stretch of interfacial water. In fact, despite the assignment of the peak centered at ~3700 cm^{-1} in vSFG spectra obtained from the air/water interface[33] and alumina/water[6] to the free OH stretch, several reports have assigned the peak with ν > 3600 cm^{-1} in vSFG spectra obtained at alumina/water interfaces to the hydroxyl group of Al_2O_3.[9,23,24] Additionally, in one report by the Shen group, one type of hydroxyl group ($AlOH_2$) appeared at 3490 cm^{-1} in the vSFG spectrum.[22] This variability in assignments makes the interpretation of frequency domain vSFG measurements open for debate.

In order to assign the high-frequency peak centered at 3650 cm^{-1} in Figure 1, we carried out time domain vSFG measurements to probe the nature of these vibrational modes, using two independently tunable ultrabroadband optical parametric amplifiers (NOPA1 and NOPA2). Because the low-frequency peak (ν < 3500 cm^{-1}) is spectrally separated from the high-frequency peak (ν > 3500 cm^{-1}) in the frequency domain vSFG spectrum (Figure 1), an independent measurement of the dephasing times of high-frequency vibrational modes can be made by tuning the sub-40 fs mid-IR pulse, the idler output of NOPA1, to excite only the high-frequency modes displayed in the vSFG spectrum (Figure 1). After a controlled time delay, $\Delta\tau$, a short upconverting NIR pulse, the signal output of NOPA2, probes the remaining coherence by generating a polarization at the NIR sum frequency (ω_{NIR} + $\omega_{\text{mid-IR}}$).

In order to characterize the temporal resolution of the FID-SFG, NIR-SFG cross-correlation traces between the mid-IR pulse and the NIR upconverting pulse were recorded (Figure 2). Qualitatively, the NIR-SFG spectra at different time delays (Figure 2a) show negligible temporal chirp. Quantitatively, this is expressed by the nearly constant position of the center of mass (CoM) at ~930 nm in NIR-SFG spectra when the time

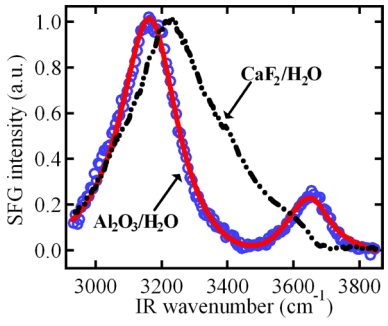

Figure 1. Normalized Vis-SFG spectrum obtained at the Al_2O_3/H_2O (pH = 13, KOH) interface (symbol plot) fit to eq 1 (solid line). Normalized Vis-SFG spectrum obtained at the CaF_2/H_2O (pH = 13, KOH) interface (dashed plot).

dx.doi.org/10.1021/jz401961j | J. Phys. Chem. Lett. 2014, 5, 528−533

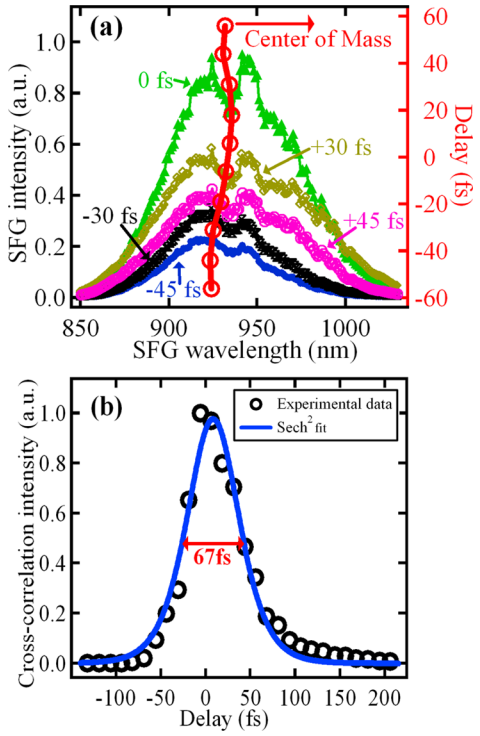

Figure 2. NIR-SFG spectra and IRF from the reference sample (Al_2O_3/Au). (a) NIR-SFG spectra at different time delays as indicated. The vertical line with circles indicates the CoM of each NIR-SFG spectrum as a function of time delay. (b) NIR-SFG cross correlation of mid-IR with NIR pulses.

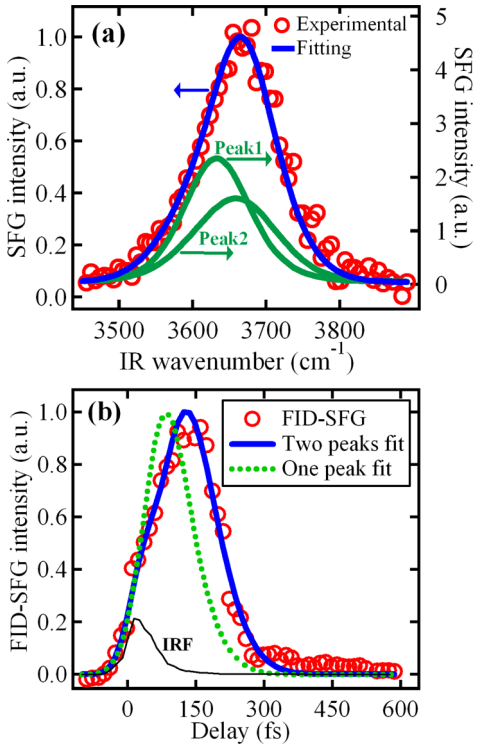

Figure 3. (a) Vis-SFG spectrum of the free OH stretch at the charged Al_2O_3/H_2O (pH ≈ 13, KOH) interface (symbols) and FID-SFG simultaneous fit (solid line). Each of the spectral components of the simultaneous fit using two oscillators is plotted by setting the amplitude of the other peak to be zero as an indication of its contribution to the spectrum. (b) FID-SFG dynamics in the spectral region of the free OH stretch at the charged Al_2O_3/H_2O (pH ≈ 13, KOH) interface (symbols) and FID-SFG simultaneous fit (solid line). The dotted line represents the simultaneous fit using one oscillator; its corresponding fit for the spectrum is shown in Figure S2a (Supporting Information). The thin solid line is the IRF, as indicated.

delay, $\Delta\tau$, changes (vertical plot in Figure 2a). The area under each NIR-SFG spectrum was plotted as a function of $\Delta\tau$ to produce the instrument response function (IRF) plotted in Figure 2b. The IRF has fwhm = 67 ± 2.5 fs and is fit well by a sech^2 function (solid line in Figure 2b). Assuming that the mid-IR and NIR pulses have similar durations,[27] the extracted pulse durations are on the order of ~39 fs, assuming sech^2 shaped pulses.

In principle, the frequency domain and time domain SFG measurements are equivalent and are related to each other by Fourier transform.[25,34] Due to spectral resolution limitations, time domain measurements (FID-SFG) are desirable when sufficient temporal resolution, signal-to-noise ratio, and delay range are available. The spectral width of the high-frequency peak, centered at ~3650 cm^{-1}, in the frequency domain vSFG spectrum (Figure 1 and Table 1) suggests that the dephasing time is on the order of 70 fs. This time scale is longer than the IRF extracted from NIR-SFG cross correlation shown in Figure 2b.

The measured FID-SFG dynamics at the Al_2O_3/H_2O (pH ≈ 13, KOH) interface in the high-frequency range (ν > 3500 cm^{-1}) are shown in Figure 3b. In order to correlate these measurements with the frequency domain vSFG spectrum (Figure 3a), we carried out a simultaneous fit[17,18] of the two sets of data (Figure 3). The nonexponential decay in the experimental FID-SFG dynamics shown in Figure 3b is an indication of the broadening of the homogeneous line width by an inhomogeneous contribution.[18,25] This suggests the addition of an inhomogeneous line width (Γ_{inh}) to the homogeneous line width (Γ_n) for each vibrational mode. The new fit function, eq 2, for the Vis-SFG spectrum used in the simultaneous fit contains a sum of convolutions (conv) of a Gaussian and a Lorentzian for each resonant feature to account for the inhomogeneous broadening and can be written as[18]

$$I_{SFG} \propto \left| \sum_n \mathrm{conv}\left(\frac{A_n}{\omega_{\text{mid-IR}} - \omega_n + i(\Gamma_n + \Delta\omega_{Vis}/2)} \times \exp\left\{ -\left(\frac{\omega_{\text{mid-IR}} - \omega_n}{\Gamma_{\text{inh},n}} \right)^2 \right\} \right) + \frac{|A_{NR}|}{\Delta\omega_{\text{mid-IR}}} e^{i\varphi} \right|^2 \times \exp\left\{ -\left(\frac{\omega_{\text{mid-IR}} - \omega_0}{\Delta\omega_{\text{mid-IR}}} \right)^2 \right\} \quad (2)$$

with ω_0 and $\Delta\omega_{\text{mid-IR}}$ as the center frequency and width of the mid-IR pulse, respectively.

Table 1. Amplitude, Frequency, and Line Width of the *n*th Mode from a Fit by Equation 1 of the Vis-SFG Spectrum of Al_2O_3/H_2O (pH ≈ 13, KOH) Shown in Figure 1[a]

A_n	ω_n (cm^{-1})	Γ_n (cm^{-1})
+77.5	3165.6	77.5
+22.0	3644.6	76.9

[a]The values of A_{NR} and ϕ were 0.24 and $-\pi/2$, respectively.

dx.doi.org/10.1021/jz401961j | J. Phys. Chem. Lett. 2014, 5, 528−533

Table 2. Amplitude, Frequency, Homogeneous Line Width, Homogeneous Dephasing Time, and Inhomogeneous Broadening Extracted from the Simultaneous Fit of the SFG Spectrum and the FID-SFG of Al_2O_3/H_2O (pH ≈ 13, KOH) in the ν > 3500 cm^{-1} Spectral Region[a]

A_n	ω_n (cm^{-1})	Γ_n (cm^{-1})	$T_{2,n}$ (fs)	$\Gamma_{inh,n}$ (cm^{-1})
−0.26 ± 0.02	3644 ± 15	5.8 ± 0.5	924 ± 79	35.2 ± 4.6
+0.24 ± 0.03	3679.4 ± 8.0	59.7 ± 4.7	89.6 ± 6.9	41.6 ± 0.5

[a]Homogeneous dephasing time $T_{2,n}$ is extracted from Γ_n as $T_{2,n} = 1/(2\pi\Gamma_n)$.[17] Errors bars are based on the standard deviation determined from multiple experiments.

For fitting the FID-SFG dynamics, the following equation was used

$$I_{\text{FID-SFG}}(\Delta\tau) \propto \int_{-\infty}^{\infty} dt\ |P^{(2)}(t, \Delta\tau)|^2 \tag{3a}$$

$$P^{(2)}(t, \Delta\tau) \propto E_{\text{NIR}}(t - \Delta\tau)P^{(1)}(t) \tag{3b}$$

$$P^{(1)}(t) = \int_{-\infty}^{\infty} dt'\ E_{\text{mid-IR}}(t - t')R(t') \tag{3c}$$

where the second-order polarization $P^{(2)}$ at a given time delay, $\Delta\tau$, expressed in eq 3b is created by mixing the first-order polarization $P^{(1)}$ induced by the mid-IR excitation ($E_{\text{mid-IR}}$) and the polarization induced by the NIR upconverting field (E_{NIR}) as expressed in eq 3c

$$R(t) = \{\delta(t)|A_{\text{NR}}|\exp(i\varphi) - i\theta(t) \sum_n A_{\text{R},n} \times \exp[2\pi c(-i\omega_n t - \Gamma_n t)] \times \exp(-2\pi c\Gamma_{\text{inh},n}t)^2\} + \text{c.c.} \tag{3d}$$

Equation 3d describes the response of the system, $R(t)$, where $\delta(t)$ is the delta function, $\theta(t)$ is the Heaviside step function, and c is the speed of light. Γ_n and Γ_{inh} are the half-width at half-maximum (HWHM) of the homogeneous and inhomogeneous line widths, respectively, of the nth vibrational mode.[17] During the simultaneous fit of the Vis-SFG spectra and the FID-SFG dynamics, the result of which is shown in Figure 3, the phase, homogeneous line width, inhomogeneous line width, and center frequency of each vibrational mode in eqs 2 and 3a are linked to each other.

As the frequency domain vSFG results suggested, we tried to carry out the simultaneous fit using one peak. Although the simulation described well the vSFG spectrum (Figure S2a in the Supporting Information), it did not account for the FID-SFG dynamics (Figure 3b). However, a two-peak simultaneous fit described well both the vSFG spectrum and the FID-SFG dynamics (Figure 3). The converged fit returned the parameters listed in Table 2.

The FID-SFG dynamics shown in Figure 3b and the simultaneous fit parameters listed in Table 2 suggest the presence of two oscillators close in frequency that oscillate with opposite phases, implying two distinct types of OH groups oriented in opposite directions to each other. This is manifested in the behavior of the rising side of the dynamics. At early delay, the increase in FID-SFG intensity is rapid; it follows the instantaneous IRF. Then, at about $\Delta\tau \approx 40$ fs, the rate of NIR-SFG intensity increase slows down. This is due to the fact that the two oscillators, which are close in frequency and of comparable strength and opposite phases, begin to cancel each other.

On the basis of several reports, the free OH stretch of interfacial water appears at 3700 cm^{-1} at the water/air interface[33] and red shifts by 20 cm^{-1} at the water/octadecyltrichlorosilane/silica (H_2O/OTS/SiO_2) interface.[19] Therefore, it is likely that the peak centered at 3679 cm^{-1} (Figure 3 and Table 2) is due to the free OH stretch of interfacial water. The fact that its broadening is dominated by a homogeneous line width, unlike the peak centered at 3644 cm^{-1}, suggests that the interfacial water species that contribute to the free OH stretch are relatively well ordered. Its homogeneous dephasing time is on the order of 90 fs, which is surprisingly fast compared to the estimated value, $T_2 \approx 300$ fs, based on frequency domain measurements at H_2O/OTS/SiO_2.[35] The peak centered at ∼3644 cm^{-1} has negative amplitude (Table 2), which indicates, following arguments by Shen et al. based on phase-sensitive vSFG measurements, that this O−H is pointing away from the bulk alumina.[9] Consequently, we assign it to the dangling OH stretch of an alumina hydroxyl group, for example, Al_2OH. Its line width is dominated by inhomogeneous broadening, and it dephases on the 0.9 ps time scale.

According to reports by the Shen group[9,22] and the Dhinojwala group,[23,24] there are several types of AlOH groups that show up at several frequencies in vSFG spectra. In fact, the Shen group reported that at the protonated interface of air/alumina ($1\bar{1}02$), there are three types of hydroxyl groups, one from Al_3OH at 3365 cm^{-1} and two from $AlOH_2$ at 3670 and 3520 cm^{-1}, corresponding to dangling and H-bonded OHs, respectively.[22] In another report by the Shen group,[9] the $(Al)_nOH$ hydroxyl group peak is assigned at 3700 cm^{-1} in the vSFG spectrum of the water/alumina(0001) interface. Furthermore, in two reports by the Dhinojwala group,[23,24] the hydroxyl group shows up at 3720 cm^{-1} in the vSFG spectrum of the water/alumina (0001) interface. On the basis of these different reports,[9,22−24] it seems that OH vibrational stretches of alumina hydroxyl groups appear at different frequencies depending on the plane of alumina under investigation. In this work, we used an alumina surface, (1120), that had not been investigated previously. Therefore, it is not unexpected that the dangling OH stretch of the Al_2OH hydroxyl group appeared at a different frequency.

Surface SFG was employed in both the frequency and the time domains to study the free OH vibrational stretching mode at Al_2O_3/H_2O (pH ≈ 13, KOH) interface. Frequency domain studies suggested the presence of two vibrational modes, a strongly hydrogen bonded OH stretch centered at 3166 cm^{-1} and a high-frequency band centered at ∼3660 cm^{-1}. NIR and mid-IR pulses with durations on the order of 40 fs were employed to carry out time domain vSFG studies. Simultaneous fit of the time domain and the frequency domain vSFG data suggested that the high-frequency band (ν > 3500 cm^{-1}) is actually composed of two vibrational modes, one mode centered at ∼3679 cm^{-1}, attributed to a free OH stretch of interfacial water, which dephases in the ∼90 fs time scale, and one mode assigned to one type of aluminum hydroxyl group, centered at ∼3644 cm^{-1}, which is characterized by homoge-

dx.doi.org/10.1021/jz401961j | J. Phys. Chem. Lett. 2014, 5, 528−533

neous dephasing on the 900 fs time scale. A full understanding of the vibrational dynamics of hydrogen bonding at the interface of alumina/water may require a systematic study, such as the alumina surface plane dependence.

EXPERIMENTAL SECTION

Sample Preparation. Alumina hemicylindrical prisms (13 mm diameter and 27 mm length) were purchased from Meller Optics. Before the experiment, the prism was cleaned in concentrated sulfuric acid for 3 min and rinsed with deionized water (>18.2 MΩ·cm resistivity) continuously for 5 min. Immediately after rinsing, the prism was dried for 5 min under continuous exposure to compressed nitrogen gas. The solution was prepared by adding potassium hydroxide (KOH, purchased from Fisher scientific) to deionized water until a pH of 13 is achieved. The KOH salt was previously baked for 24 h at a temperature of 260 °C.

The alumina prism plane identification was done following the reported procedure using X-ray diffraction.[36,37] A similar hemicylinder alumina prism was coated with a ∼100 nm thick gold film[31] and used for spectral and temporal characterization of mid-IR and NIR pulses.

Frequency and Time Domain SFG Setup. The experimental setup for carrying out SFG in the frequency domain and the time domain has been described elsewhere in detail.[27] Briefly, it is based on a Ti:sapphire oscillator (MIRA, Coherent) laser source, which is regeneratively amplified with a BMI Thales (Alpha 1000) laser system operating in fs mode, as described elsewhere.[38] The output pulse is centered at 800 nm with a 150 fs duration at a 1 kHz repetition rate and an energy per pulse of 600 μJ. The regenerative amplifier output is used to pump two NOPAs; NOPA1 is used to generate ultrashort mid-IR pulses, and NOPA2 is used to generate ultrashort upconverting pulses in the NIR for FID-SFG measurements. As described in detail elsewhere,[31] NOPA1 generates a mid-IR idler in a two-stage amplification sequence; the first stage uses a lithium niobate (LNB) crystal, and the second stage is potassium niobate (KNB)-based. The mid-IR output of NOPA1 was collimated by a 50 mm CaF_2 lens, passed through a 1 mm thick Si long pass filter to cutoff residual signal and white light continuum (WLC) after the second stage, and then focused onto the Al_2O_3/H_2O interface using a 50 mm CaF_2 lens at a 73° angle of incidence. Because the mid-IR is spectrally broad (fwhm > 600 cm^{-1}), its propagation through these optics causes temporal chirp. In order to compensate for this chirp and temporally compress the mid-IR pulse to sub-40 fs duration, a 5 mm thick Si window was introduced into the optical path of the mid-IR pulse.[27]

For frequency domain SFG measurements, the 800 nm output of the regenerative amplifier was used to upconvert the mid-IR pulses into the visible by sum frequency generation (Vis-SFG). For better spectral resolution, the 800 nm beam was passed through a narrow-band filter (NBF) to spectrally narrow it down to ∼2−2.3 nm (∼30−37 cm^{-1}), consequently stretching its pulse duration to ∼500 fs.[39]

In order to carry out time domain SFG measurements (FID-SFG) with temporal resolution sufficient to resolve sub-50 fs vibrational dynamics, a NIR ultrashort pulse was generated in NOPA2 and used to upconvert mid-IR pulses into a NIR sum frequency field (NIR-SFG).[27] Briefly, less than 10 μJ of the fundamental laser was focused using a 100 mm focal length BK7 lens on a 2 mm thick sapphire window for WLC generation; the WLC was collimated using a 100 mm focal length BK7 lens before being focused on a potassium titanium oxide phosphate (KTP) crystal using a 250 mm focusing BK7 lens. To pump the crystal, about 100 μJ of the 800 nm fundamental was focused onto the KTP crystal with a 500 mm BK7 lens at a noncollinear angle of 7° with respect to the WLC seed.[27] The signal output of NOPA2, tunable in the 1100−1600 mm spectral range, was collimated by a 250 mm CaF_2 lens, and residual WLC and fundamental (800 nm) were filtered out using silicon wafers (1 mm total thickness) set at the Brewster angle (73°). The collimated signal of NOPA2 was temporally compressed using two Brewster fused silica prisms (P1 and P2) set at their Brewster angle (69.6°) and separated by a distance of 290 mm. The dispersion in the signal of NOPA2, caused by propagation through optics before reaching the studied interface, was compensated for by the appropriate distance between P1 and P2 and the amount of P1 and P2 inserted in the beam.[27] The spectrum and autocorrelation traces of the NIR signal output of NOPA2 are shown in Figure S1 (Supporting Information).

Depending on the experiment, an ultrashort NIR pulse or narrow-band visible pulse was sent through a motorized delay stage before it was focused with a 100 mm CaF_2 lens and overlapped with the mid-IR pulse at the Al_2O_3/H_2O interface at a 55° angle of incidence. At the sample, pulse energies were 4, 2, and 10 μJ for mid-IR, NIR, and 800 nm pulses, respectively.

The reflected Vis-SFG or NIR-SFG (depending on the experiment) beam was collimated and then focused into a 200 μm core fiber coupled with a spectrograph-CCD (Andor Shamrock/iDus) detection system. The Vis-SFG and FID-SFG signals were recorded using a custom-built program based on Labview software (National Instruments). Using half-wave plates and polarizers, the SFG, the NIR, the 800 nm upconverting pulses, and the mid-IR were p-polarized relative to the interface. We checked that p-polarized input beams emerge essentially p-polarized after reflection from the sample, suggesting that, despite the birefringence of sapphire, the polarization is maintained.

Time zero, $\Delta\tau_0$, for FID-SFG (measured at the Al_2O_3/H_2O interface) measurements was defined as the time delay where the IRF (measured at the Al_2O_3/Au interface) intensity is maximum.

ASSOCIATED CONTENT

Supporting Information

Spectral and temporal characterization of the NIR signal output of NOPA2 and results of the simultaneous fit of SFG in frequency and time domains using one oscillator. This material is available free of charge via the Internet at http://pubs.acs.org.

AUTHOR INFORMATION

Corresponding Author

*E-mail: eborguet@temple.edu.

Author Contributions

Both authors have given approval to the final version of the manuscript.

Notes

The authors declare no competing financial interest.

ACKNOWLEDGMENTS

The authors acknowledge the National Science Foundation for supporting this work (NSF Grant CHE 1337880). The authors thank Professor M. Zdilla for alumina prism face orientation identification by X-ray diffraction and Mr. Steve Szewczyk at

the University of Pennsylvania, Department of Materials Science and Engineering for gold coating of the alumina prism.

REFERENCES

(1) Geissler, P. L. Water Interfaces, Solvation, and Spectroscopy. *Annu. Rev. Phys. Chem.* **2013**, *64*, 317−337.
(2) Chaplin, M. Do We Underestimate the Importance of Water in Cell Biology? *Nat. Rev. Mol. Cell Biol.* **2006**, *7*, 861−866.
(3) Berne, B. J.; Weeks, J. D.; Zhou, R. Dewetting and Hydrophobic Interaction in Physical and Biological Systems. *Annu. Rev. Phys. Chem.* **2009**, *60*, 85−103.
(4) Nihonyanagi, S.; Mondal, J. A.; Yamaguchi, S.; Tahara, T. Structure and Dynamics of Interfacial Water Studied by Heterodyne-Detected Vibrational Sum-Frequency Generation. *Annu. Rev. Phys. Chem.* **2013**, *64*, 579−603.
(5) Dontsova, K. M.; Norton, L. D.; Johnston, C. T.; Bigham, J. M. Influence of Exchangeable Cations on Water Adsorption by Soil Clays. *Soil Sci. Soc. Am. J.* **2004**, *68*, 1218−1227.
(6) Yeganeh, M. S.; Dougal, S. M.; Pink, H. S. Vibrational Spectroscopy of Water at Liquid/Solid Interfaces: Crossing the Isoelectric Point of a Solid Surface. *Phys. Rev. Lett.* **1999**, *83*, 1179−1182.
(7) Maeda, K.; Domen, K. Photocatalytic Water Splitting: Recent Progress and Future Challenges. *J. Phys. Chem. Lett.* **2010**, *1*, 2655−2661.
(8) Dewan, S.; Yeganeh, M. S.; Borguet, E. Experimental Correlation Between Interfacial Water Structure and Mineral Reactivity. *J. Phys. Chem. Lett.* **2013**, *4*, 1977−1982.
(9) Zhang, L.; Tian, C.; Waychunas, G. A.; Shen, Y. R. Structures and Charging of α-Alumina (0001)/Water Interfaces Studied by Sum-Frequency Vibrational Spectroscopy. *J. Am. Chem. Soc.* **2008**, *130*, 7686−7694.
(10) Eftekhari-Bafrooei, A.; Borguet, E. Effect of Surface Charge on the Vibrational Dynamics of Interfacial Water. *J. Am. Chem. Soc.* **2009**, *131*, 12034−12035.
(11) Fecko, C. J.; Eaves, J. D.; Loparo, J. J.; Tokmakoff, A.; Geissler, P. L. Ultrafast Hydrogen-Bond Dynamics in the Infrared Spectroscopy of Water. *Science* **2003**, *301*, 1698−1702.
(12) Cowan, M. L.; Bruner, B. D.; Huse, N.; Dwyer, J. R.; Chugh, B.; Nibbering, E. T. J.; Elsaesser, T.; Miller, R. J. D. Ultrafast Memory Loss and Energy Redistribution in the Hydrogen Bond Network of Liquid H_2O. *Nature* **2005**, *434*, 199−202.
(13) Crowell, R. A.; Holtom, G. R.; Xie, X. S. Infrared Free Induction Decay of Liquid Water Molecules. *J. Phys. Chem.* **1995**, *99*, 1840−1842.
(14) Piletic, I. R.; Moilanen, D. E.; Levinger, N. E.; Fayer, M. D. What Nonlinear-IR Experiments Can Tell You about Water That the IR Spectrum Cannot. *J. Am. Chem. Soc.* **2006**, *128*, 10366−10367.
(15) Fayer, M. D. Dynamics of Water Interacting with Interfaces, Molecules, and Ions. *Acc. Chem. Res.* **2012**, *45*, 3−14.
(16) Fayer, M. D.; Levinger, N. E. Analysis of Water in Confined Geometries and at Interfaces. *Annu. Rev. Anal. Chem.* **2010**, *3*, 89−107.
(17) Nihonyanagi, S.; Eftekhari-Bafrooei, A.; Borguet, E. Ultrafast Vibrational Dynamics and Spectroscopy of a Siloxane Self-Assembled Monolayer. *J. Chem. Phys.* **2011**, *134*, 084701−7.
(18) Eftekhari-Bafrooei, A.; Nihonyanagi, S.; Borguet, E. Spectroscopy and Dynamics of the Multiple Free OH Species at an Aqueous/Hydrophobic Interface. *J. Phys. Chem. C* **2012**, *116*, 21734−21741.
(19) Shen, Y. R.; Ostroverkhov, V. Sum-Frequency Vibrational Spectroscopy on Water Interfaces: Polar Orientation of Water Molecules at Interfaces. *Chem. Rev.* **2006**, *106*, 1140−1154.
(20) Ball, P. How to Keep Dry in Water. *Nature* **2003**, *423*, 25−26.
(21) Shen, Y. R. *The Principles of Nonlinear Optics*; Wiley: New York, 1984.
(22) Sung, J.; Zhang, L.; Tian, C.; Shen, Y. R.; Waychunas, G. A. Effect of pH on the Water/α-Al_2O_3 (1102) Interface Structure Studied by Sum-Frequency Vibrational Spectroscopy. *J. Phys. Chem. C* **2011**, *115*, 13887−13893.
(23) Anim-Danso, E.; Zhang, Y.; Dhinojwala, A. Freezing and Melting of Salt Hydrates Next to Solid Surfaces Probed by Infrared−Visible Sum Frequency Generation Spectroscopy. *J. Am. Chem. Soc.* **2013**, *135*, 8496−8499.
(24) Anim-Danso, E.; Zhang, Y.; Alizadeh, A.; Dhinojwala, A. Freezing of Water Next to Solid Surfaces Probed by Infrared−Visible Sum Frequency Generation Spectroscopy. *J. Am. Chem. Soc.* **2013**, *135*, 2734−2740.
(25) Roke, S.; Kleyn, A. W.; Bonn, M. Time- vs. Frequency-Domain Femtosecond Surface Sum Frequency Generation. *Chem. Phys. Lett.* **2003**, *370*, 227−232.
(26) Guyot-Sionnest, P. Coherent Processes at Surfaces: Free-Induction Decay and Photon Echo of the Si−H Stretching Vibration for H/Si(111). *Phys. Rev. Lett.* **1991**, *66*, 1489−1492.
(27) Boulesbaa, A.; Isaienko, O.; Borguet, E. Generation of Sub-30 fs Microjoule Mid-Infrared Pulses for Ultrafast Vibrational Dynamics at Solid/Liquid Interfaces. *Opt. Lett.* **2013**, *38*, 5008−5011.
(28) Brida, D.; Manzoni, C.; Cirmi, G.; Marangoni, M.; Bonora, S.; Villoresi, P.; De Silvestri, S.; Cerullo, G. Few-Optical-Cycle Pulses Tunable from the Visible to the Mid-Infrared by Optical Parametric Amplifiers. *J. Opt.* **2010**, *12*, 013001.
(29) Isaienko, O.; Borguet, E. Generation of Ultra-Broadband Pulses in the Near-IR by Non-Collinear Optical Parametric Amplification in Potassium Titanyl Phosphate. *Opt. Express* **2008**, *16*, 3949−3954.
(30) Brida, D.; Marangoni, M.; Manzoni, C.; De Silvestri, S.; Cerullo, G. Two-Optical-Cycle Pulses in the Mid-Infrared from an Optical Parametric Amplifier. *Opt. Lett.* **2008**, *33*, 2901−2903.
(31) Isaienko, O.; Borguet, E. Ultra-Broadband Sum-Frequency Vibrational Spectrometer of Aqueous Interfaces Based on a Non-Collinear Optical Parametric Amplifier. *Opt. Express* **2012**, *20*, 547−561.
(32) Liu, H.; Mu, G.; Lin, L.; Fan, Z. Pulse Compression beyond the Fourier-Transform Limit. *J. Opt. Soc. Am. A* **2006**, *23*, 848−857.
(33) Raymond, E. A.; Tarbuck, T. L.; Brown, M. G.; Richmond, G. L. Hydrogen-Bonding Interactions at the Vapor/Water Interface Investigated by Vibrational Sum-Frequency Spectroscopy of HOD/H_2O/D_2O Mixtures and Molecular Dynamics Simulations. *J. Phys. Chem. B* **2003**, *107*, 546−556.
(34) Bordenyuk, A. N.; Jayathilake, H.; Benderskii, A. V. Coherent Vibrational Quantum Beats as a Probe of Langmuir−Blodgett Monolayers. *J. Phys. Chem. B* **2005**, *109*, 15941−15949.
(35) McGuire, J. A.; Shen, Y. R. Ultrafast Vibrational Dynamics at Water Interfaces. *Science* **2006**, *313*, 1945−1948.
(36) Kikuchi, T. Single Crystal Orientation Measurement by X-ray Methods. *Rigaku J.* **1990**, *7*, 27−35.
(37) Hildebrandt, G.; Bradaczek, H. High Precision Crystal Orientation Measurements with the X-ray Omega-Scan — A Tool for the Industrial Use of Quartz and Other Crystals. *J. Optoelectron. Adv. Mater.* **2004**, *6*, 5−21.
(38) Bodlaki, D.; Borguet, E. Picosecond Infrared Optical Parametric Amplifier for Nonlinear Interface Spectroscopy. *Rev. Sci. Instrum.* **2000**, *71*, 4050−4056.
(39) Lagutchev, A.; Lozano, A.; Mukherjee, P.; Hambir, S. A.; Dlott, D. D. Compact Broadband Vibrational Sum-Frequency Generation Spectrometer with Nonresonant Suppression. *Spectrochim. Acta Mol. Biomol. Spectrosc.* **2010**, *75*, 2010.